

# $\alpha 6$ -Containing GABA<sub>A</sub> Receptors Are the Principal Mediators of Inhibitory Synapse Strengthening by Insulin in Cerebellar Granule Cells

Michael V. Accardi,<sup>1,2</sup> Patricia M.G.E. Brown,<sup>1,3</sup> Loïs S. Miraucourt,<sup>1</sup> Beverley A. Orser,<sup>4</sup> and  Derek Bowie<sup>1</sup>

<sup>1</sup>Department of Pharmacology and Therapeutics, <sup>2</sup>Graduate Program in Pharmacology, and <sup>3</sup>Integrated Program in Neuroscience, McGill University, Montréal, Québec H3A 2B4, Canada, and <sup>4</sup>Department of Physiology, University of Toronto, Toronto, Ontario M5S 1A8, Canada

Activity-dependent strengthening of central synapses is a key factor driving neuronal circuit behavior in the vertebrate CNS. At fast inhibitory synapses, strengthening is thought to occur by increasing the number of GABA<sub>A</sub> receptors (GABARs) of the same subunit composition to preexisting synapses. Here, we show that strengthening of mouse cerebellar granule cell GABAergic synapses occurs by a different mechanism. Specifically, we show that the neuropeptide hormone, insulin, strengthens inhibitory synapses by recruiting  $\alpha 6$ -containing GABARs rather than accumulating more  $\alpha 1$ -containing receptors that are resident to the synapse. Because  $\alpha 6$ -receptors are targeted to functionally distinct postsynaptic sites from  $\alpha 1$ -receptors, we conclude that only a subset of all inhibitory synapses are strengthened. Together with our recent findings on stellate cells, we propose a general mechanism by which mature inhibitory synapses are strengthened. In this scenario,  $\alpha 1$ -GABARs resident to inhibitory synapses form the hardwiring of neuronal circuits with receptors of a different composition fulfilling a fundamental, but unappreciated, role in synapse strengthening.

**Key words:** inhibition; insulin; metabolism; mitochondria; plasticity mechanism; reactive oxygen species

## Introduction

Fast inhibitory transmission in the adult vertebrate CNS is primarily mediated by a family of ligand-gated ion-channels called GABA<sub>A</sub> receptors (GABARs) that stabilize the membrane potential by transporting chloride and bicarbonate ions (Belelli et al., 2009; Miller and Smart, 2010; Rudolph and Knoflach, 2011). GABARs assemble as a pentameric anion channel most commonly composed of 2  $\alpha$  ( $\alpha 1$ – $\alpha 6$ ) and 2  $\beta$  ( $\beta 1$ – $\beta 3$ ) subunits with an additional subunit, typically a  $\gamma$  ( $\gamma 1$ – $\gamma 3$ ) subunit that may be replaced with a  $\delta$ ,  $\epsilon$ , or  $\theta$  subunit (Barnard et al., 1998; Moss and Smart, 2001; Rudolph et al., 2001). This richness in subunit diversity is a central factor in determining many aspects of GABAR signaling. For example, switches in subunit composition are commonly observed during neuronal development fulfilling roles in differentiation and maturation (Fritschy and Panzanelli, 2006). In cerebellar granule and stellate cells, there is a develop-

mental change in the kinetics of synaptic events with slower rates ( $\tau_{(fast)}$ , 9–19 ms) observed in migrating P7–P11 neurons (Tia et al., 1996; Vicini et al., 2001) that express  $\alpha 1$ – $\alpha 3$  and  $\alpha 6$  subunits (Laurie et al., 1992a, b), respectively. In adult P20–P35 neurons, however, synaptic events become faster ( $\tau_{(fast)}$ , 6–7 ms) (Tia et al., 1996; Vicini et al., 2001) due to the dominant expression of  $\alpha 1$ -containing GABARs (Somogyi et al., 1996; Vicini et al., 2001). Despite the prevalence of  $\alpha 1$ -receptors in adult synapses, stellate and granule neurons continue to express  $\alpha 2/3$ - and  $\alpha 6$ -containing receptors, respectively (Laurie et al., 1992a, b; Persohn et al., 1992; Tia et al., 1996; Vicini et al., 2001) whose role, if any, in signaling at the synapse is unclear.

Although numerous effector molecules strengthen inhibitory synapses, each is thought to change synaptic efficacy by increasing the number of GABARs per synapse (e.g., Otis et al., 1994; Nusser et al., 1997). It is generally assumed that inhibitory synapses are strengthened by the recruitment of GABARs of the same composition, more often than not, due to  $\alpha 1$ -containing receptors given their predominance in the adult CNS (Luscher et al., 2011; Rudolph and Knoflach, 2011). However, recent work from our laboratory has revealed that mitochondrial-derived reactive oxygen species (mROS) strengthen inhibitory synapses of cerebellar stellate cells by a mechanism distinct in two important ways. First, synapse strengthening is mediated by the recruitment of  $\alpha 3$ -containing receptors and not resident  $\alpha 1$ -receptors (Accardi et al., 2014). Second,  $\alpha 3$ -receptors are targeted to functionally separate postsynaptic sites from  $\alpha 1$ -receptors (Accardi et al., 2014), implying that not all synapses are strengthened by mROS. Whether this novel mechanism is unique to stellate cells or more

Received Feb. 5, 2015; revised May 4, 2015; accepted May 28, 2015.

Author contributions: M.V.A., P.M.G.E.B., L.S.M., B.A.O., and D.B. designed research; M.V.A., P.M.G.E.B., and L.S.M. performed research; M.V.A., P.M.G.E.B., L.S.M., and D.B. analyzed data; M.V.A., P.M.G.E.B., L.S.M., and D.B. wrote the paper.

This work was supported by Canadian Institutes of Health Research Operating Grants FRN:82804 to D.B. and MOP:416838 and MOP:480143 to B.A.O., M.V.A. was supported by a studentship from the Savoy Foundation. P.M.G.E.B. was supported by a doctoral fellowship from Fonds de la Recherche en Santé du Québec. D.B. and B.A.O. are the recipients of a Canada Research Chair award. We thank members of the D.B. laboratory, especially Dr. Bryan Daniels and Brent Dawe, for discussions and comments on the manuscript.

The authors declare no competing financial interests.

Correspondence should be addressed to Dr. Derek Bowie, Department of Pharmacology and Therapeutics, Bellini Building, Room 164, McGill University, 3649 Promenade Sir William Osler, Montreal, Quebec H3G 0B1, Canada. E-mail: derek.bowie@mcgill.ca.

DOI:10.1523/JNEUROSCI.0513-15.2015

Copyright © 2015 the authors 0270-6474/15/359676-13\$15.00/0

commonly used throughout the CNS remains to be investigated. On that note, recruitment of  $\alpha 3$ -containing GABARs causes a slowing in decay kinetics of synaptic events (Accardi et al., 2014), an observation not observed in other studies (Otis et al., 1994; Luscher et al., 2011). This distinction raises the possibility that mROS have a unique effect on stellate cell inhibitory synapses that is not found elsewhere.

To address this issue directly, we have studied the mechanism by which ROS strengthen inhibitory synapses of cerebellar granule cells: the most abundant neuron in the vertebrate brain (Llinás, 1969). ROS was elevated by perfusing the mitochondrial uncoupler, antimycin-A, via the patch electrode or by bath application of the metabolic hormone, insulin. Like in stellate cells, ROS augment inhibitory synaptic transmission of granule cells by recruiting receptors of a different subunit composition, in this case,  $\alpha 6$ -containing GABARs, to postsynaptic sites that are distinct from resident  $\alpha 1$ -receptors. Unlike in stellate cells, however, synapse strengthening is not accompanied by a slowing of synaptic events. Together, we conclude that  $\alpha 1$ -containing GABARs form the hardwiring of inhibitory synapses of stellate and granule cells with  $\alpha 3$ - or  $\alpha 6$ -containing GABARs fulfilling a fundamental but unexpected role as the principal mediators of GABAergic synapse strengthening.

## Materials and Methods

**Animals.** Breeder pairs for homozygous GABAR  $\delta$ -knock-out (*Gabrd*<sup>-/-</sup>;  $\delta$ -KO) mice were generously provided by Dr. Gregg Homanics (University of Pittsburgh) and bred at the University of Toronto for experimentation.  $\delta$ -KO mice were generated using a background of C57BL/6  $\times$  Sv129Ev mice as described previously (Mihalek et al., 1999). Wild-type mice were maintained on a C57BL/6J background (Charles River Laboratories) and maintained as a breeding colony at both McGill University (Montreal, Quebec, Canada) and University of Toronto (Toronto, Ontario, Canada). All KO animals were genotyped by PCR analysis of tail biopsies. Mice (Wild-type and  $\delta$ -KO: male and female) used for the experiments ranged from postnatal day 15 to 28 (P15–P28; mean  $\pm$  SEM age: P21  $\pm$  1,  $n$  = 51). All experiments have been approved by the local authorities, were performed in accordance with the guidelines of the Canadian Council on Animal Care, and were approved by the Animal Care Committee of McGill University and University of Toronto.

**Cerebellum slice preparation.** Mice were anesthetized with isoflurane and immediately decapitated. The cerebellum was rapidly removed from the whole brain while submerged in oxygenated (95% O<sub>2</sub>, 5% CO<sub>2</sub>) ice-cold cutting solution, which contained (in mM) as follows: 235 sucrose, 2.5 KCl, 1.25 NaH<sub>2</sub>PO<sub>4</sub>, 28 NaHCO<sub>3</sub>, 0.5 CaCl<sub>2</sub>, 7 MgSO<sub>4</sub>, 28 D-glucose (pH 7.4; 305–315 mOsmol/L). The tissue was maintained in ice-cold solution while sagittal slices of cerebellar vermis (300  $\mu$ m) were cut using a vibrating tissue slicer (Leica VT100S, Leica Instruments). The slices were transferred to oxygenated aCSF and held at room temperature (20°C–23°C) for at least 1 h before recordings were performed. aCSF contained the following (in mM): 125 NaCl, 2.5 KCl, 1.25 NaH<sub>2</sub>PO<sub>4</sub>, 26 NaHCO<sub>3</sub>, 2 CaCl<sub>2</sub>, 1 MgSO<sub>4</sub>, 25 D-glucose (pH of 7.4; 305–315 mOsmol/L).

**Electrophysiology.** Slice experiments were performed on an Olympus BX51 upright microscope (Olympus) equipped with differential interference contrast/infrared optics. Whole-cell patch-clamp recordings were performed on granule cells located in the granule cell layer, which were visually identified based on cell body size and were confirmed *post hoc* by imaging with Lucifer yellow. Patch pipettes were prepared from thick-walled borosilicate glass (GC150F-10, OD 1.5 mm, ID 0.86 mm; Harvard Apparatus) and had open tip resistances of 6–12 M $\Omega$  when filled with an intracellular solution that contained (in mM) as follows: 140 CsCl, 4 NaCl, 0.5 CaCl<sub>2</sub>, 10 HEPES, 5 EGTA, 2 Mg-ATP, and 2 QX314 to block voltage-activated Na<sup>+</sup> channels with 0.5 mg/ml Lucifer yellow as a *post hoc* dye indicator (pH 7.4 with CsOH, 300–310 mOsmol/L). Recordings were made with a Multiclamp 700A amplifier (Molecular Devices)

in voltage-clamp mode with a holding potential of  $-60$  mV. Series resistance and whole-cell capacitance were estimated by cancelling the fast current transients evoked at the onset and offset of brief (10–20 ms) 5 mV voltage-command steps. Series resistance during whole-cell recording (10–35 M $\Omega$ ) was compensated between 40% and 65% and checked for stability throughout the experiments (>20% tolerance). The capacitance of the granule cells was in the range of 1.5–4 pF. The bath was continuously perfused at room temperature (22°C–23°C) with aCSF at a rate of 1–2 ml/min. Miniature IPSCs (mIPSCs) were recorded in the presence of TTX (1  $\mu$ M). Currents were filtered at 5 kHz with an eight-pole low-pass Bessel filter (Frequency Devices) and digitized at 25 kHz with a Digidata 1322A data acquisition board and Clampex9 (Molecular Devices) software. Data acquisition was performed using pClamp9 and pClamp10 software (Molecular Devices). Curve fitting and figure preparation of all electrophysiology data were performed with Origin 7.0 (OriginLab), Microsoft Excel, Clampfit 10 (Molecular Devices), and the Strathclyde Electrophysiology WinWCP and WinEDR (John Dempster) software.

mIPSCs from granule cells occur too infrequently to permit a proper characterization of their response characteristics in terms of event amplitude and decay times (Wall and Usowicz, 1997). In view of this, we performed all experiments in aCSF with elevated extracellular K<sup>+</sup> (18 mM), as described by others (Momiya and Takahashi, 1994), which significantly increased baseline frequency approximately eightfold from  $0.07 \pm 0.01$  Hz (aCSF, 2.5 mM KCl,  $n$  = 5) to  $0.54 \pm 0.01$  Hz (aCSF, 18 mM KCl,  $n$  = 5;  $p$  = 0.0001, unpaired Student's  $t$  test). Other than the change in mIPSC frequency, all other characteristics (i.e., distribution of rise times, amplitudes, and decay kinetics) were indistinguishable between experiments in 2.5 and 18 mM K<sup>+</sup> aCSF solutions. This was also true with mice exposed to the internal perfusion of antimycin-A (aCSF, 2.5 mM KCl,  $n$  = 6:  $0.13 \pm 0.03$  Hz; aCSF, 18 mM KCl,  $n$  = 4:  $1.04 \pm 0.25$ ;  $p$  = 0.002, unpaired Student's  $t$  test) as well as  $\delta$ -KO animals (aCSF, 2.5 mM KCl,  $n$  = 6:  $0.13 \pm 0.04$  Hz; aCSF, 18 mM KCl,  $n$  = 5:  $1.7 \pm 0.2$ ;  $p$  = 0.0001, unpaired Student's  $t$  test). Consequently, we concluded that the use of an elevated extracellular K<sup>+</sup> aCSF solution was a useful tool for increasing mIPSC frequency. aCSF (18 mM K<sup>+</sup>) was only used as an external bathing solution during electrophysiological recordings and not during the recovery period before experimentation. To account for the increase in osmotic pressure with aCSF (18 mM K<sup>+</sup>), sucrose was added to the internal pipette solution to achieve isomolarity (330 mOsmol/L).

Experiments were also performed at room temperature on recombinant GABARs 24–48 h after cDNA transfection. GABA (Sigma-Aldrich) was dissolved in external solution containing the following (in mM): 150 NaCl, 5 HEPES, 2 MgCl<sub>2</sub>, and 1 CaCl<sub>2</sub>. Internal pipette solution contained the following (in mM): 150 KCl, 5 EGTA, 1 MgCl<sub>2</sub>, and 2 Mg-ATP. The pH and osmotic pressure of internal and external solutions were adjusted to 7.3–7.4 and 300 mOsmol<sup>-1</sup>, respectively. Furosemide was dissolved as a 100 mM stock in DMSO, stored at  $-20^\circ\text{C}$ , and diluted to a final concentration of 100  $\mu$ M in external solutions. The control external solution also contained an equal amount of DMSO (0.1% v/v). Control and agonist solutions were rapidly applied to outside-out patches excised from transfected HEK 239T/17 cells using a piezoelectric stack (Physik Instrumente). Solution exchange (10%–90% rise-time = 150–250  $\mu$ s) was determined in a separate experiment by measuring the liquid junction current (or exchange current) between the control and external solution containing 10% additional NaCl. All recordings were performed with an Axopatch 200B amplifier (Molecular Devices) using thin-walled borosilicate glass pipettes (2–5 M $\Omega$ ) coated with dental wax to reduce electrical noise. Current records were filtered at 5 kHz, digitized at 25 kHz, and series resistances (3–10 M $\Omega$ ) were compensated by 95%. All recordings were performed at a holding potential of  $-60$  mV.

**Analysis of mIPSC events.** mIPSCs were detected using WinEDR software with a detection threshold of  $4 \times$  the mean square root of noise level. The accuracy of detection was visually confirmed for each event in each recording. Amplitude distributions were fit with the sum of 2–3 Gaussian functions with the singular form of the following:  $y = (A/(\pi w)) * \exp(-2 * ((x - xc)/w)^2)$ , where  $A$  is the area,  $xc$  is the center of the peak, and  $w$  is the error associated with the peak. The decay phase of mIPSCs was fit with a single exponential curve, and both rise and

decay phases were fitted between 10% and 90% of the peak amplitude. Data are expressed as mean  $\pm$  SEM. *p* values represent the results obtained from either a paired or unpaired, two-tailed Student's *t* tests or a one-way ANOVA with Tukey's *post hoc* test. A *p* value of  $<0.05$  was considered statistically significant. All data are from at least two different animals.

**Intracellular ROS fluorescence.** Slices for imaging experiments were incubated in oxygenated aCSF containing CM-H<sub>2</sub>DCF-DA (5  $\mu$ M DCF, Invitrogen) 45 min before imaging cytosolic ROS levels using a Zeiss Axioexaminer upright microscope (Carl Zeiss) equipped with a multiphoton chameleon (coherent) laser source set to excite at 780 nm (power = 0.3 W/cm<sup>2</sup>). To visualize changes in DCF fluorescence intensity, XYZT series images of the cerebellar granule cell layer were acquired every 2 min using a 40 $\times$  plan apochromatic objective (NA = 1.0). After baseline imaging (10 min), another 30 min of imaging followed, during which various drugs (insulin, 0.5  $\mu$ M and/or genistein, 50  $\mu$ M) were applied through the constant flow of oxygenated aCSF (1.5 ml/min). Slices during genistein treatment were incubated for  $\sim$ 45 min in aCSF + genistein (together with DCF) before the start of the 10 min baseline imaging. Images were acquired on an IBM-compatible computer using Zen software (Carl Zeiss) and subsequently analyzed using NIH Image/ImageJ.

**Fluorescence image analysis.** To analyze the change in fluorescence intensity, one or two focal planes of respective matching depth (*z*-axis) in every XYZ stacks were selected. Twenty ROIs were drawn per focal plane, to each surround individual granule cell soma (minimal XY drift was corrected using the ImageJ registration plugin). Raw measurements of all ROIs (mean pixel intensity) were used to perform Gaussian distributions of fluorescence intensity among the different groups (*n* = 3 slices for control; *n* = 4 slices for insulin; *n* = 4 slices for insulin + genistein). To compare the change of fluorescence intensity over time among groups, the  $\Delta$ fluorescence of each ROI ( $\Delta F = F_t - F_0$ , where  $F_0$  is the mean ROI fluorescence during the first 10 min of the experiment) was determined. This analysis was restricted to granule cells (or ROIs) for which  $F_t$  did not vary  $>10\%$  of  $F_0$  during the first 10 min, to ensure a stable baseline before insulin application.

**Pharmacological compounds.** Ionotropic glutamate receptor antagonists, D-APV (for NMDARs; 10  $\mu$ M) and CNQX (for non-NMDARs; 5  $\mu$ M), the glycine receptor antagonist, strychnine (0.3  $\mu$ M) and the GABAR antagonist bicuculline (10  $\mu$ M) were purchased from Tocris Bioscience. TTX (1  $\mu$ M) was purchased from Alomone Labs). Stock solutions of these antagonists were prepared in water and were stored at  $-20^\circ\text{C}$ , and working solutions were diluted with aCSF shortly before application to the bath. The antioxidant, *N*-acetylcysteine (NAC, 1 mM) (Sigma) was prepared as a stock solution (100 mM) in water and dissolved in patch electrode solution on the day of the experiment. The mitochondrial uncoupler, antimycin-A (2  $\mu$ M), was purchased from Sigma, dissolved in DMSO, and diluted in water to workable stock concentrations and stored at  $-20^\circ\text{C}$ . The final maximum external DMSO concentration (0.1% v/v) had no effect on mIPSCs, consistent with other studies (Nakahiro et al., 1992). Mg-ATP (2 mM) was included in our patch electrode solution to maintain cytoplasmic ATP levels. Furosemide (100  $\mu$ M; Tocris Bioscience) was dissolved in DMSO, stored at  $-20^\circ\text{C}$ , and added directly into the aCSF on the day of the recordings. Although not significant (*p* = 0.27, paired Student's *t* test), furosemide application produced a small increase in mIPSC frequency of  $\sim 29\%$  (22.5 min; see Fig. 4D, *n* = 5) immediately following the introduction of furosemide to the bath, an effect also observed by others (Mark Farrant, personal communication). Nevertheless, this change in mIPSC frequency was not sustained and returned to basal levels within 5–10 min. Insulin (0.5  $\mu$ M, Sigma) was prepared from a 163  $\mu$ M stock that required 0.1 M acetic acid to ensure complete dissolution. The concentration of insulin used is consistent with previous studies and also corresponds to circulating hormone levels (Wozniak et al., 1993; Wan et al., 1997). Genistein (50  $\mu$ M; Tocris Bioscience), the protein tyrosine kinase and insulin receptor antagonist, was completely dissolved in DMSO and stored at  $-20^\circ\text{C}$  at a final concentration of 50 mM. The phosphatidylinositol 3-kinase (PI3-kinase) inhibitor, wortmannin (1  $\mu$ M; Tocris Bioscience), was dissolved in DMSO, diluted in water to a stock concentration of 500  $\mu$ M, and stored

at  $-20^\circ\text{C}$ . The final maximum internal pipette DMSO concentration was  $<0.1\%$  v/v.

## Results

### Mitochondrial ROS strengthens GABAergic synapses of cerebellar granule cells

To study the mechanism that strengthens GABAergic synapses, whole-cell recordings of mouse cerebellar granule cells were performed with an internal pipette solution containing the mitochondrial uncoupler, antimycin-A (2  $\mu$ M, Fig. 1). Prior work from our laboratory on cerebellar stellate cells has established that antimycin-A and other uncouplers strengthen GABAergic transmission by elevating mROS (Accardi et al., 2014). We reasoned that they would have a similar effect on granule cells. In agreement with this, internal patch perfusion with antimycin-A elicited an increase in the frequency of inhibitory synaptic events by almost 1.5-fold during a typical 20–25 min recording (0–5 min,  $0.74 \pm 0.33$  Hz; 20–25 min,  $1.04 \pm 0.25$  Hz; *n* = 4, *p* = 0.036, paired two-tailed Student's *t* test; Fig. 1A–C), an observation absent from control recordings (Fig. 1D). Gaussian fits of the amplitude distributions revealed that antimycin-A selectively increased the occurrence of only mIPSCs of small amplitude with little effect on larger-amplitude events (Fig. 1A, B). For example, fits of the smallest events were 28% of all events within 0–5 min (Fig. 1A, bottom), which increased 1.5-fold, to 41%, after 20–25 min (Fig. 1B, bottom). As a consequence, we observed a small time-dependent reduction in the averaged amplitude of mIPSCs (e.g., 0–5 min,  $-38.3 \pm 6.0$  pA; 20–25 min,  $-31.2 \pm 2.8$  pA; 17% reduction; Fig. 1C, D), similar to our observations on stellate cells (Accardi et al., 2014). The increase in mIPSC frequency is due to an elevation in cytosolic mROS because the effect of antimycin-A was attenuated by inclusion of the antioxidant, NAC (1 mM, *n* = 4), in the patch electrode solution (*p* < 0.01, one-way ANOVA; Fig. 1D). Interestingly, we also observed an effect of antimycin-A on tonic GABA current baseline (25 min after seal breakthrough, Control, *n* = 5,  $20.46 \pm 4.7$  pA; Antimycin-A, *n* = 6,  $3.46 \pm 0.93$  pA; *p* = 0.004; unpaired Student's *t* test), suggesting that mROS also affect extrasynaptic receptors. These observations are similar to our earlier findings on cerebellar stellate cells suggesting that mROS are a common intermediary that couple cellular metabolism to the processes that strengthen GABAergic signaling.

mROS may strengthen GABAergic transmission by a presynaptic and/or postsynaptic mechanism. In stellate cells, the effect of mROS is abolished in mice lacking the  $\alpha 3$  GABAR subunit (Accardi et al., 2014), which is primarily located in the perisynaptic and/or extrasynaptic space (Fritschy and Panzanelli, 2006). As a result, we concluded that mROS strengthen inhibitory transmission primarily by a postsynaptic mechanism via the recruitment of  $\alpha 3$ -containing GABARs into the synapse (Accardi et al., 2014). A similar mechanism may be at play in granule cells because mROS selectively augment the occurrence of inhibitory events of small amplitude (Fig. 1A, B) in a similar manner previously reported in stellate cells. Granule cells, however, do not express  $\alpha 3$  subunits and thus may strengthen inhibitory transmission by recruiting any one of several GABARs. Adult granule cells express GABARs composed of  $\alpha 1/\beta 2, 3/\gamma 2$ ,  $\alpha 6/\beta 2, 3/\gamma 2$ , and/or  $\alpha 1, 6/\beta 2, 3/\gamma 2$  at their synapses, whereas  $\alpha 6/\beta 2, 3/\gamma 2$ ,  $\alpha 1, 6/\beta 2, 3/\gamma 2$ , and  $\alpha 6/\beta 2, 3/\delta$  GABARs are found outside the synapse (Nusser et al., 1995, 1996, 1998a; Mapelli et al., 2014). Because only  $\gamma 2$ -containing receptors are capable of entering synapses (Luscher et al., 2011), we concluded mROS do not mediate their effects by recruiting  $\alpha 6/\beta 2, 3/\delta$  receptors. In agreement with this, bath application of Zn<sup>2+</sup> (10  $\mu$ M) elicited no noticeable reduc-

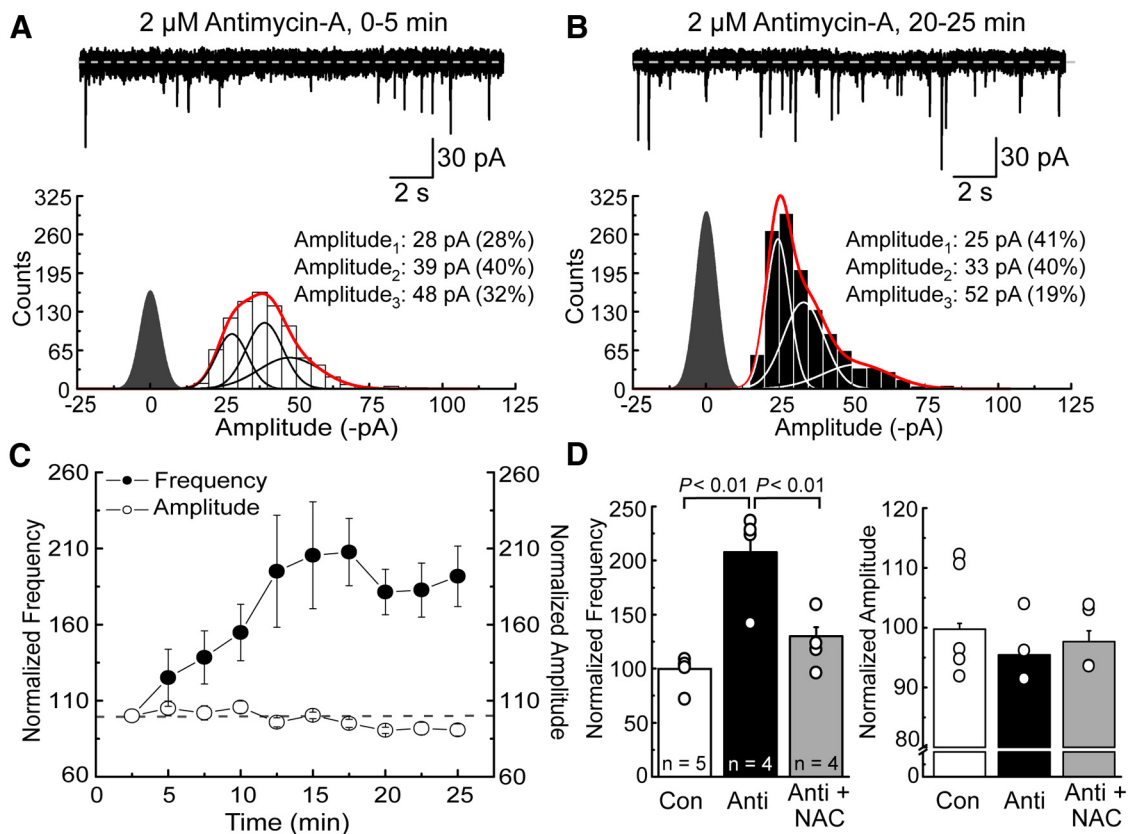


**Figure 1.** mROS selectively increase the occurrence of inhibitory events of small amplitude. *A, B*, Top, mIPSCs from the same granule cell (cell #140307000) at the beginning (0–5 min) and during (20–25 min) pipette perfusion with antimycin-A (2  $\mu$ M). Bottom, Amplitude histograms comparing the data obtained at two time periods (i.e., 0–5 min, left; 20–25 min, right,  $n = 4$ ). Each was fit with the sum of three Gaussian functions (red line), with individual functions shown in either black (left panel) or white (right panel). In this figure and elsewhere, the closed point distribution (filled; dark gray) was scaled to the fitted peak of the lowest event amplitude and represents the average baseline noise observed during the recordings. *C*, Summary plot of the time course of mIPSC frequency (filled circle) and amplitude (open circle) during pipette perfusion with antimycin-A. Data are mean  $\pm$  SEM. *D*, Bar graphs of maximal normalized frequency (left) and amplitude (right) obtained in the different recording conditions. Anti, antimycin-A; NAC, *N*-acetylcysteine (1 mM). Statistical test was a one-way ANOVA with Tukey's *post hoc* test. The frequency comparison of "Control" versus "Anti + NAC" (*D*; left) was not significant and, for clarity, was not indicated in the figure. Amplitude comparisons were not significant ( $p = 0.58$ ; one-way ANOVA).

tion on mIPSC amplitude (normalized: without  $Zn^{2+}$ ,  $n = 4$ , 20–25 min:  $90.7 \pm 4.0\%$ ; with  $Zn^{2+}$ ,  $n = 5$ , 20–25 min:  $100.6 \pm 6.4\%$ ;  $p = 0.26$ ; unpaired Student's *t* test) or frequency (normalized: without  $Zn^{2+}$ ,  $n = 4$ , 20–25 min:  $207.65 \pm 22.1\%$ ; with  $Zn^{2+}$ ,  $n = 5$ , 20–25 min:  $201.96 \pm 15.7\%$ ;  $p = 0.84$ ; unpaired Student's *t* test) induced by antimycin-A. Because  $Zn^{2+}$  blocks GABARs that do not contain the  $\gamma 2$  subunit (May and de Haën, 1979; Draguhn et al., 1990), we concluded that the effect of mROS on mIPSC frequency was not mediated through the recruitment of extrasynaptic  $\delta$ -containing GABARs.

To explore the potential involvement of  $\alpha 1$ - and/or  $\alpha 6$ -containing GABARs, we looked for ways to discriminate between them at GABAergic synapses. Pharmacological studies on native and recombinant GABARs have reported that furosemide will selectively block  $\alpha 6$ -containing receptors (Korpi et al., 1995; Tia et al., 1996; Minier and Sigel, 2004). To confirm this, we first examined the degree of furosemide block on recombinant GABARs containing either  $\alpha 1$  or  $\alpha 6$  subunits where subunit composition would be known (Fig. 2; Table 1). Next, we determined the degree of furosemide block of native GABARs where the contribution of  $\alpha 6$ -containing GABARs is not known (Fig. 2*A*, right). Accordingly, we reasoned that a greater degree of block of mIPSCs would correspond to a greater presence of  $\alpha 6$ -containing receptors at GABAergic synapses.

As reported previously (Tia et al., 1996), 100  $\mu$ M furosemide had almost no effect on the peak response amplitude or deactivation kinetics of  $\alpha 1$ -containing GABARs (Fig. 2*A, B*; Table 1). In contrast, however, furosemide reduced the peak response amplitude and affected deactivation kinetics of  $\alpha 6$ -containing GABARs (Fig. 2*A*; Table 1). Given these two effects, the charge transfer mediated by  $\alpha 6$ -containing GABARs was significantly reduced to  $46 \pm 9\%$  ( $n = 5$ ,  $p = 0.009$ , paired Student's *t* test) of the control in the presence of furosemide (100  $\mu$ M; Fig. 2*B*; Table 1), demonstrating that furosemide is an ideal pharmacological agent to discriminate between the contribution of  $\alpha 1$ - or  $\alpha 6$ -containing GABARs. Interestingly, bath application of furosemide (100  $\mu$ M) produced a modest effect on peak mIPSC amplitudes (Peak<sub>before</sub>,  $-43 \pm 2.2$  pA; Peak<sub>after</sub>,  $-34 \pm 2.3$  pA,  $p = 0.03$ , paired Student's *t* test) that was not statistically significant for charge transfer (Fig. 2*A, B*;  $p = 0.10$ , paired Student's *t* test), underscoring the minimal contribution of  $\alpha 6$ -containing GABARs under control conditions. Furthermore, a comparison of mIPSC decay kinetics revealed the time-dependent occurrence of some synaptic events with slower decay kinetics (i.e.,  $\geq 20$  ms) during antimycin-A treatment (Fig. 2*C*, filled symbol). Although these slower events were too few in number to affect the overall decay kinetics of mIPSCs from granule cells (Fig. 2*A*, right), it is consistent with the possibility that mROS recruit  $\alpha 6$ -containing

GABARs, which have slower gating behavior (Fig. 2A, middle; Table 1).

In summary, these data highlight that  $\alpha$ 1- and  $\alpha$ 6-containing receptors can be distinguished by their sensitivity to block by furosemide. We therefore reasoned that, if mROS strengthen GABAergic synapses by the recruitment of  $\alpha$ 6-containing receptors, furosemide should block or attenuate the effect of antimycin-A on mIPSC frequency.

### Pharmacological block of $\alpha$ 6-containing GABARs abolishes synapse strengthening

To test this possibility, cerebellar slices were bathed in furosemide (100  $\mu$ M) before and during whole-cell recordings from granule cells with internal perfusion of antimycin-A (Fig. 3). As expected, preincubation with furosemide had a modest effect on mIPSC baseline frequency and amplitude (Fig. 2A,B), consistent with our assertion that granule cell inhibitory synapses contain a small proportion of  $\alpha$ 6-containing GABARs. For example, baseline mIPSC frequency in slices before and after furosemide application were  $0.96 \pm 0.22$  Hz and  $0.87 \pm 0.18$  Hz ( $p = 0.46$ ; paired Student's *t* test;  $n = 6$ ), respectively. Interestingly, internal perfusion with antimycin-A had no detectable effect on mIPSC frequency (0–5 min,  $1.08 \pm 0.28$  Hz; 20–25 min,  $1.15 \pm 0.088$  Hz;  $p = 0.78$ ; paired Student's *t* test,  $n = 6$ ) (Fig. 3A–D) in marked contrast to its effects on naive slices (Fig. 1C,D). Moreover, fits of mIPSC amplitude distributions revealed that antimycin-A did not elicit a time-dependent increase in the occurrence of mIPSCs of events with small amplitude (Fig. 3A–C). Data obtained during the first 5 min of recording were best fit with the sum of 2 Gaussian functions with peak values of  $-29 \pm 0.15$  pA (81%) and  $-41 \pm 1.3$  pA (19%), which were indistinguishable from the peak values of  $-26 \pm 0.15$  pA (75%) and  $-38 \pm 0.92$  pA (25%) obtained in the last 5 min (i.e., 20–25 min) (Fig. 3C). These data are therefore consistent with the assertion that antimycin-A strengthens inhibitory synapses of granule cells by recruiting  $\alpha$ 6-containing GABARs.

Like all loop diuretics, furosemide acts on the anion/cation transporters, such as NKCC2 (Haas and Forbush, 1998) and KCC2 (Payne, 1997), but may have other pharmacological targets. Therefore, an immediate concern was that our observations may reflect furosemide's action on more than just  $\alpha$ 6-containing GABARs. We ruled out an effect on anion/cation transporters because transmembrane anion/cation gradients are constrained in the whole-cell recording configuration and because block usually occurs at concentrations greater than that used in the present study (Misgeld et al., 1986). To exclude the possibility of other targets, and provide additional evidence for the recruitment of  $\alpha$ 6-containing GABARs, we performed two separate experiments. First, we tested whether furosemide would exert a greater pharmacological block of mIPSCs after granule cells were treated with antimycin-A because mROS would be expected to recruit more  $\alpha$ 6-containing receptors into the synapse (Fig. 4). Second,

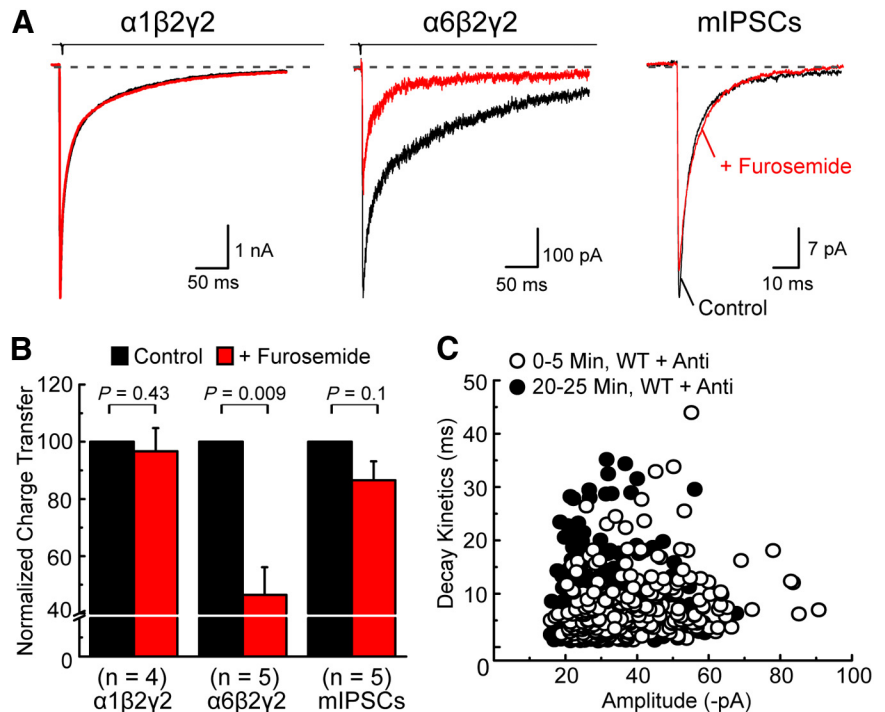


**Figure 2.** Furosemide block distinguishes between  $\alpha$ 1- and  $\alpha$ 6-containing GABA<sub>A</sub> receptors. **A**, Overlay of typical membrane currents elicited by short 1 ms applications of 10 mM GABA on recombinant  $\alpha$ 1 $\beta$ 2 $\gamma$ 2 (left, patch #141219p8;  $n = 4$ ) and  $\alpha$ 6 $\beta$ 2 $\gamma$ 2 (middle, patch #141219p3;  $n = 5$ ) or averaged mIPSC from a granule cell (right, cell #140605000;  $n = 5$ ) before (black line) and after (red line) bath application of 100  $\mu$ M furosemide. **B**, Bar graph comparing the degree of furosemide block on charge transfer between recombinant and native GABARs. Data are mean  $\pm$  SEM, with paired Student's *t* tests and Bonferroni correction. **C**, Plot comparing mIPSC amplitude versus decay kinetics observed in the first 5 min (0–5 min, open circles) and last 5 min (20–25 min, filled circles) of recording in antimycin-A (2  $\mu$ M).

we reasoned that furosemide would have a greater pharmacological block on mIPSCs of granule cells lacking the  $\delta$ -subunit (Fig. 5) because mice lacking this subunit have been noted to have an upregulated expression of  $\alpha$ 6-containing GABARs (Tretter et al., 2001).

### Furosemide block of $\alpha$ 6-containing GABARs is more pronounced after antimycin-A treatment

Experiments comparing furosemide block of mIPSCs in control and antimycin-A-treated granule cells are summarized in Figure 4. In all cases, furosemide induced a significant reduction of the baseline membrane noise (compare Fig. 4A, top and bottom) consistent with antagonism of extrasynaptic  $\alpha$ 6- (and  $\delta$ -) containing receptors. This effect represents a  $>50\%$  reduction in baseline current for control (Pre-Furosemide,  $14.36 \pm 1.9$  pA; Post-Furosemide,  $6.93 \pm 0.66$  pA;  $p = 0.017$ ; paired Student's *t* test;  $n = 5$ ) and antimycin-A (53% reduction, Pre-Furosemide,  $13.39 \pm 0.94$  pA; Post-Furosemide,  $6.30 \pm 0.54$  pA;  $p = 0.0074$ ; paired Student's *t* test;  $n = 5$ ) conditions. In control granule cells, furosemide had a modest effect on mIPSC amplitude and almost no effect on mIPSC frequency (Fig. 4A,B left, D). In contrast, furosemide had a significant effect on mIPSC amplitude and frequency after antimycin-A treatment (Fig. 4A,B right, C,D). mIPSC amplitude was reduced by  $\sim 40\%$  with 100  $\mu$ M furosemide ( $p = 0.0007$ ; paired Student's *t* test), representing an almost twofold greater block than control conditions (Fig. 4B right, D). Most strikingly, the increase in mIPSC frequency induced by antimycin-A was completely abolished following bath application of 100  $\mu$ M furosemide (Fig. 4C,D). mIPSC frequency at 20–25 min was  $1.43 \pm 0.15$  Hz compared with  $0.87 \pm 0.074$  Hz at 40–45 min when block by furosemide had reached equilib-

**Table 1. Kinetics of  $\alpha 1\beta 2\gamma 2$  and  $\alpha 6\beta 2\gamma 2$  GABA<sub>A</sub> receptors (1 ms pulse, 10 mM GABA)**

	Components	t1 (mean ± SEM)	% A1	t2 (mean ± SEM)	% A2	t3 (mean ± SEM)	% A3	n
<b><math>\alpha 1\beta 2\gamma 2</math></b>								
Control	3	2.7 ± 0.2	29	21.2 ± 2.4	39	130.1 ± 11.9	32	4
+ 100 $\mu$ M furosemide	3	2.0 ± 0.2	31	19.8 ± 3.1	37	150.8 ± 19.5	32	4
<b><math>\alpha 6\beta 2\gamma 2</math></b>								
Control	3	3.5 ± 0.4	16	23.1 ± 4.0	41	196.0 ± 5.1	43	5
+ 100 $\mu$ M furosemide	3	6.4 ± 1.5	36	27.0 ± 3.7	48	337.9 ± 50.8	16	5

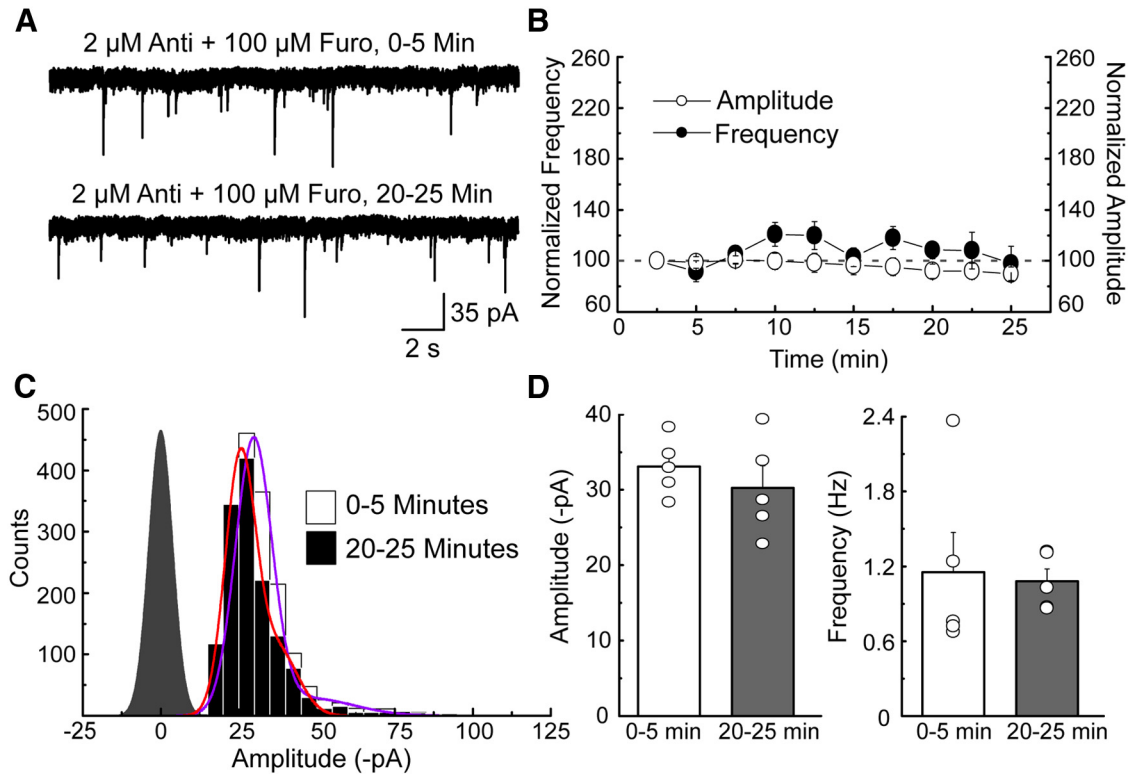


**Figure 3.** Pharmacological block of  $\alpha 6$ -containing GABA<sub>A</sub> receptors prevents synaptic strengthening by mROS. **A**, mIPSCs from two time points (cell #140329013) from the same cell during bath application of furosemide (100  $\mu$ M) and internal perfusion with antimycin-A (2  $\mu$ M). **B**, Plot summarizing the effect of antimycin-A on event frequency (filled circle) and amplitude (open circle) ( $n = 5$ ). **C**, Amplitude histograms of data from the same cells at two time points fit with the sum of 2 Gaussian functions (purple represents 0–5 min; red represents 20–25 min). **D**, Bar graphs comparing the effect of furosemide on mIPSC amplitude (left) and frequency (right) during internal patch perfusion with antimycin-A. In all cases, data are mean ± SEM.

rium (Fig. 4C,D). Indeed, mIPSC frequency was statistically indistinguishable ( $p = 0.46$ ; paired Student's  $t$  test,  $n = 6$ ) between measurements at the beginning (i.e., 0–5 min,  $0.96 \pm 0.091$  Hz) and end (i.e., 40–45 min,  $0.87 \pm 0.074$  Hz) of the experiment (Fig. 4C,D). These data support the assertion that strengthening of granule cell GABAergic synapses by mROS is due to the recruitment of  $\alpha 6$ -containing GABARs. As discussed below, we further tested the involvement of  $\alpha 6$ -containing GABARs by studying the effect of antimycin-A on granule cells that lack the  $\delta$ -subunit.

**Antimycin-A fails to strengthen GABAergic synapses of granule cells from  $\delta$ -KO mice**

Previous studies have shown that the overall surface expression of the  $\alpha 6$ -subunit is unchanged in granule cells from  $\delta$ -KO mice but that there is an increased surface expression of the  $\gamma 2$ -subunit (Tretter et al., 2001), presumably because of a compensatory mechanism. Given this, we reasoned that granule cell inhibitory synapses would contain more  $\alpha 6/\gamma 2$ -containing GABARs, as proposed by others previously (Tretter et al., 2001). In keeping with this, we observed an increased basal frequency of mIPSCs by

approximately twofold to threefold in  $\delta$ -KO mice ( $n = 5$ ) compared with wild-type ( $\delta$ -KO:  $1.69 \pm 0.20$  Hz; wild-type:  $0.543 \pm 0.087$  Hz;  $p = 0.0008$ ; unpaired Student's  $t$  test) consistent with an upregulation of inhibitory synaptic connections. More importantly, bath application of 100  $\mu$ M furosemide elicited a much greater reduction in both mIPSC amplitude and frequency in granule cells from  $\delta$ -KO than wild-type mice (Fig. 5). For instance, furosemide reduced mIPSC frequency in wild-type granule cells from  $0.96 \pm 0.22$  Hz to  $0.87 \pm 0.18$  Hz, which was much more modest than the effect in  $\delta$ -KO mice where mIPSC frequency was reduced from  $1.7 \pm 0.2$  Hz to  $0.60 \pm 0.19$  Hz (Fig. 5B,D). Likewise, peak mIPSC amplitudes were reduced by ~20% in wild-type granule cells compared with a reduction of ~31% in granule cells lacking the  $\delta$ -subunit (Fig. 5B–D). Together, these observations make two important conclusions regarding granule cells of  $\delta$ -KO mice: (1) they exhibit a greater number of functional inhibitory synapses; and (2) inhibitory synapses contain a greater proportion of  $\alpha 6/\gamma 2$ -containing GABARs.

As a final test of the involvement of  $\alpha 6$ -containing GABARs, we examined the effect of antimycin-A on granule cells of  $\delta$ -KO mice (Fig. 5E). We reasoned that, because of the greater pro-

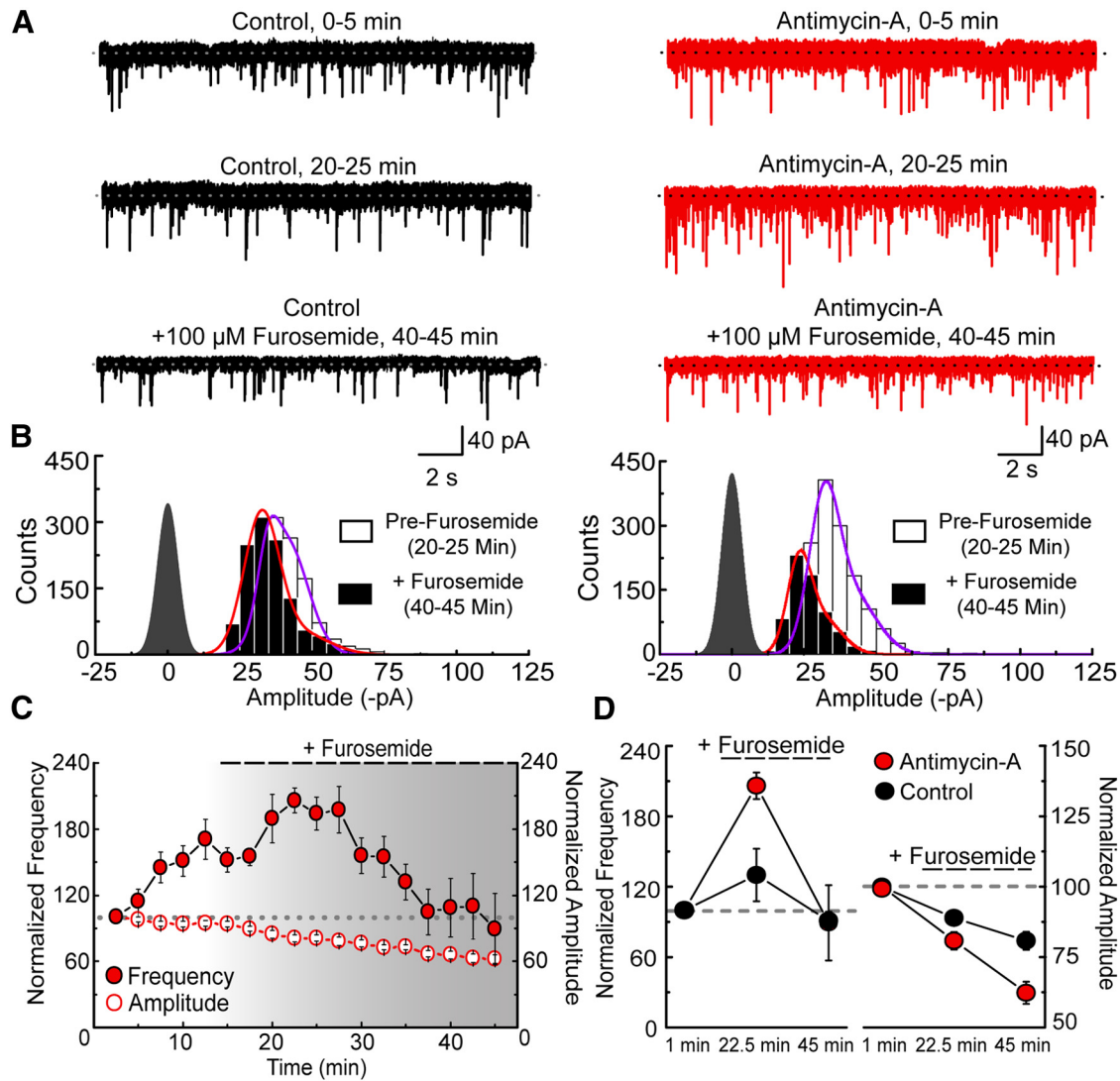


**Figure 4.** Synaptic strengthening induced by mROS is reversed by pharmacological block of  $\alpha 6$ -containing GABA<sub>A</sub> receptors. **A**, Representative electrophysiological traces of a control (left, cell #140526000) and antimycin-A (2  $\mu$ M, right, cell #140619000) treated granule cell at three separate time points. **B**, Amplitude distributions of mIPSCs from two time points ( $n = 5$  in each case). For clarity, only the summed Gaussian functions are shown (purple represents Pre-Furosemide; red represents + Furosemide). **C**, Summary plot showing the time course of mIPSC frequency (red circle) and amplitude (open circle). Furosemide (100  $\mu$ M) was added 15 min after the start of the experiment. Gray gradient represents the gradual equilibration of furosemide in the bath. **D**, Summary plots of furosemide's effect on mIPSC frequency and amplitude. Data are mean  $\pm$  SEM.

portion of  $\alpha 6/\gamma 2$ -containing GABA<sub>A</sub> receptors at these synapses, antimycin-A would have little or no effect on mIPSC frequency. That is, synapse strengthening by mROS via the recruitment of  $\alpha 6$ -containing GABA<sub>A</sub> receptors would be limited because granule cell inhibitory synapses of  $\delta$ -KO mice are already occupied by these receptors. In support of this, internal patch perfusion of antimycin-A exerted no effect on mIPSC frequency or peak amplitude (Fig. 5E). For example, mIPSC frequencies observed during the first (0–5 min) and last (20–25 min) 5 min were  $1.1 \pm 0.51$  Hz and  $1.32 \pm 0.62$  Hz, respectively ( $p = 0.35$ , paired Student's  $t$  test). Furthermore, the peaks of the fits of the antimycin-A treated  $\delta$ -KO amplitude distribution (20–25 min: Amplitude<sub>1</sub>, 37 pA; Amplitude<sub>2</sub>, 48 pA) were very similar to that of the wild-type control (20–25 min: Amplitude<sub>1</sub>, 39 pA; Amplitude<sub>2</sub>, 55 pA). These data show that antimycin-A was ineffective in strengthening GABAergic synapses of  $\delta$ -KO mice, in marked contrast to our observations on wild-type mice. We therefore conclude that strengthening of granule cell inhibitory synapses occurs by the recruitment of  $\alpha 6$ -containing GABA<sub>A</sub> receptors.

### Insulin elevates cytosolic ROS in granule cells of the mouse cerebellum

To determine whether a physiological signaling pathway strengthens GABAergic synapses in a similar manner, we examined the effect of the metabolic hormone, insulin. Prior work has established that insulin elevates cytosolic ROS (Mukherjee et al., 1978; May and de Haën, 1979; Zeng and Quon, 1996; Mahadev et al., 2001a, b; Goldstein et al., 2005) and, in separate experiments, insulin has been shown to strengthen GABAergic synapses (Wan et al., 1997; Vetiska et al., 2007). Given this, we reasoned that there may be a causal link between insulin's ability to elevate cytosolic ROS and its ability to strengthen inhibitory synapses.

To explore this, we first determined whether insulin can induce a change in the redox state of the cerebellum by loading granule cells with the fluorescent dye DCF and imaging for cytosolic ROS (Fig. 6; see Materials and Methods). Because DCF irreversibly reacts with cytosolic ROS, we anticipated that the fluorescent signal from individual cells would increase in a time-dependent manner, reflecting the constitutive turnover of their

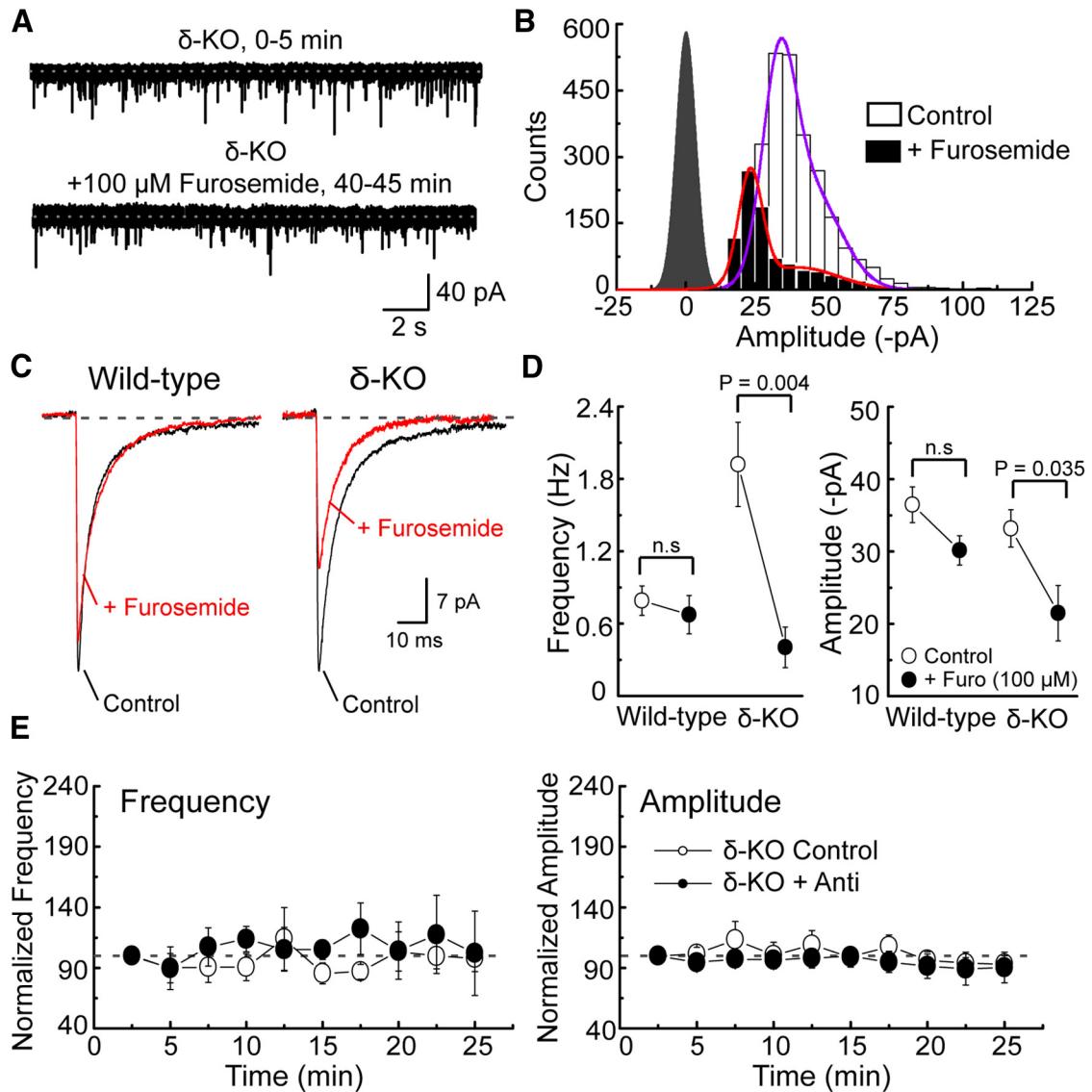


**Figure 5.** mROS fail to strengthen inhibitory synapses of  $\delta$ -KO mice. **A**, Representative recordings from a granule cell lacking the  $\delta$ -subunit before (top) and after (bottom) applying furosemide ( $100 \mu\text{M}$ , cell #140621010) to the bath 15 min after the start of the experiment. **B**, Amplitude distributions comparing mIPSCs at the two time points ( $n = 5$ ). For clarity, summed Gaussian functions are shown (purple represents Control, 0–5 min; red represents + Furosemide, 40–45 min). **C**, Averaged mIPSCs (from 15 random events) comparing the response profile of wild-type (cell #140605000) and  $\delta$ -KO (cell #1406210010) cells before (black line) and after (red line) furosemide application. **D**, Summary plot showing mIPSC frequency (left) and amplitude (right) before (“control,” open circles, 0–5 min) and after (“+ furo,” filled circle, 40–45 min) furosemide ( $100 \mu\text{M}$ ) application. Statistical test is a paired Student’s *t* test. n.s., Not significant. **E**, Summary plots showing the time course of mIPSC frequency (left) and amplitude (right) of granule cells ( $n = 5$ ) lacking the  $\delta$ -subunit in the presence (filled circle) and absence (open circle) of antimycin-A ( $2 \mu\text{M}$ ). Data are mean  $\pm$  SEM.

metabolic and signaling state. In agreement with this, we observed a gradual increase in cytosolic ROS from cerebellar slices continuously perfused with aCSF over a 30–40 min time period (Fig. 6B). Interestingly, basal ROS levels were reduced significantly by pretreatment with the isoflavone, genistein ( $50 \mu\text{M}$ ), which blocks a number of ubiquitous signaling pathways, including insulin’s actions by inhibiting tyrosine kinase activity (Fig. 6B,C). At the start of the imaging experiments, the distribution of fluorescence intensity among granule cells bathed in aCSF was fit well with a single Gaussian function with a mean amplitude of  $131 \pm 2.7$  a.u. (Fig. 6C, cyan bars), which was reduced significantly to  $35 \pm 3.5$  a.u. by genistein (Fig. 6C, black bars;  $p < 0.0001$ , unpaired Student’s *t* test). Despite this difference, the rate of change in fluorescence intensity was identical in both conditions over a typical 30–40 min imaging experiment (Fig. 6B)

demonstrating that the constitutive production of cellular ROS was constant.

As expected, basal cytosolic ROS levels observed in granule cells before insulin application were comparable with measurements made in aCSF (Fig. 6B). Upon insulin ( $0.5 \mu\text{M}$ ) application, however, we observed an almost immediate increase in cytosolic ROS generation (Fig. 6A,B) that reached statistical significance after 20 min ( $p < 0.01$ ; two-way repeated-measures ANOVA with Holm-Sidak’s multiple-comparison test). The distribution of DCF fluorescence intensity at the 24–30 min time point was fit well by the sum of two Gaussian functions with mean values of  $191 \pm 9.0$  a.u. (55%) and  $437 \pm 202$  a.u. (45%) (Fig. 6D). The emergence of a second peak, not observed in baseline recordings (Fig. 6C) or the control condition at 24–30 min (fit by a single Gaussian:  $232 \pm 5$  a.u.), highlights the presence of

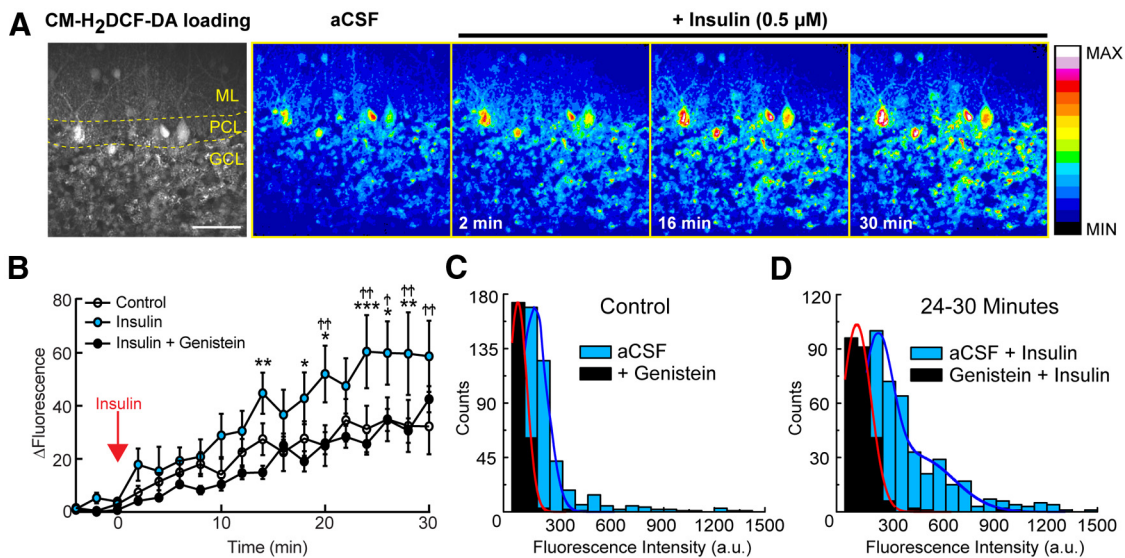


**Figure 6.** Insulin increases cytosolic ROS in cerebellar granule cells. **A**, Example DCF images from a typical insulin-treated experiment showing elevations in cytosolic ROS. The images are displayed using a color-coded map of fluorescence intensity (16 colors) ranging from black (no fluorescence), to white (maximum signal for any pixel over the course of an individual experiment). A representative two-photon single focal plane image (far left) of a cerebellar parasagittal slice with the cellular layers denoted. ML, Molecular layer; PCL, Purkinje cell layer; GCL, granule cell layer. Scale bar, 5  $\mu$ m. Right, The 16 color version of this image. **B**, Summary plot of the time course of fluorescence intensity changes in control (white circle), insulin (cyan circles), or insulin + genistein (black circles) treated conditions. Data are mean  $\pm$  SEM. Two-way repeated-measures ANOVA with Holm-Sidak's multiple-comparison test: \*Comparisons between "insulin" and "insulin + genistein." †Comparisons between "insulin" and "control." \*\* $p < 0.05$ . † $p < 0.05$ . \*\*\* $p < 0.01$ . †† $p < 0.01$ . \*\*\*\* $p < 0.001$ . **C**, Histograms comparing the level of fluorescence intensity obtained in the presence (black) or absence (cyan) of 50  $\mu$ M genistein. Each histogram was fit with a single Gaussian function (red represents genistein; dark blue represents aCSF). **D**, Histograms comparing the level of fluorescence intensity obtained after bath application of insulin (0.5  $\mu$ M) in the presence (black) or absence (cyan) of 50  $\mu$ M genistein at the end of a typical imaging recording. Each histogram was fit with either a single (red represents genistein + insulin) or the sum of two (dark blue represents aCSF + insulin), Gaussian functions.

a population of granule cells, which robustly respond to insulin. Importantly, genistein completely blocked the observed insulin-induced increase in cytosolic ROS generation (Fig. 6*B,D*), demonstrating that the action of insulin on cerebellar granule cells is due to an increase in tyrosine kinase activity. Together, these observations establish that cytosolic ROS levels in granule cells are regulated by the insulin receptor.

#### Elevating cytosolic ROS via the insulin receptor strengthens granule cell GABAergic synapses

To test for a causal relationship between ROS and strengthening of GABAergic synapses, we recorded mIPSCs from granule cells before and after bath application of insulin (0.5  $\mu$ M; Fig. 7). Similar to antimycin-A (Fig. 1), insulin elicited a time-dependent increase in mIPSC frequency by almost twofold during a typical 20–25 min recording (Fig. 7*A–C*;  $p = 0.0003$ ; paired two-tailed Student's *t* test,  $n = 11$ ). Gaussian fits of the amplitude distributions before and after insulin treatment revealed that insulin primarily increased the occurrence of mIPSCs of small amplitude with little effect on larger events (Fig. 7*A,B*). Fits of the smallest events were 19% of all events within 0–5 min (Fig. 7*A*, bottom), which increased 2.2-fold, to 42%, after 20–25 min (Fig. 7*B*, bottom), resulting in the small, time-dependent reduction in the averaged mIPSC amplitude (e.g., 0–5 min:  $-47.9 \pm 2.6$  pA; 20–25 min:  $-42 \pm 2.3$  pA; 12% reduction; Fig. 7*C,D*). Furthermore, insulin's effect on mIPSCs was almost completely abolished by including the antioxidant, NAC (1 mM,  $n = 4$ ), in the patch electrode solution ( $p < 0.01$ , one-way ANOVA; Fig. 7*D*) to diminish ROS levels. In view of this, our data establish a causal link between insulin's ability to elevate cytosolic ROS and strengthen GABAergic synapses of cerebellar granule cells.

#### Insulin recruits $\alpha 6$ -containing receptors to GABAergic synapses via a wortmannin-sensitive pathway

To test whether insulin strengthens GABAergic synapses by recruiting  $\alpha 6$ -containing receptors, we examined the ability of furosemide to reduce inhibitory transmission during insulin treatment (Fig. 8). To do this, baseline mIPSC frequency was first augmented by bath application of insulin over the first 20–25 min of the recording (Fig. 8*A,B*). In control conditions, mIPSC frequency was  $0.99 \pm 0.3$  Hz (0–5 min; Fig. 8*A*), increasing to  $1.6 \pm 0.4$  Hz (20–25 min; Fig. 8*A*) following bath application of insulin (Fig. 8*A,B*;  $p = 0.01$ ; paired Student's *t* test;  $n = 6$ ). Having established an increase in mIPSC frequency with insulin, we tested for the recruitment of  $\alpha 6$ -containing GABARs by perfusion of the  $\alpha 6$ -GABAR antagonist, furosemide (Fig. 8*B*). As anticipated, bath application of 100  $\mu$ M furosemide significantly reduced mIPSC frequency from  $1.6 \pm 0.4$  Hz (20–25 min; Fig. 8*B*) in a time-dependent manner to levels observed at the beginning of the experiment (i.e.,  $0.73 \pm 0.2$  Hz, 40–45 min,  $p = 0.03$ ; paired Student's *t* test;  $n = 6$ ) (Fig. 8*B*). Indeed, mIPSC frequency was statistically indistinguishable ( $p = 0.42$ ; paired Student's *t* test,  $n = 6$ ) between measurements observed at the beginning (i.e., 0–5 min) and end (i.e., 40–45 min) of the experiment. As expected, furosemide also had a significant effect on mIPSC amplitudes (Fig. 8*B,C*), which were reduced by  $\sim 28\%$  ( $p = 0.02$ ; paired Student's *t* test), resulting in a leftward shift in the amplitude histogram. It is noteworthy to mention that furosemide reduced the baseline membrane noise (Fig. 8*A*) by  $\sim 40\%$ , in a manner similar to that observed following antimycin-A treatment (Fig. 4), from  $11.9 \pm 0.7$  pA (Pre-Furosemide) to  $7.5 \pm 0.3$  pA (Post-Furosemide) ( $p = 0.003$ ; paired Student's *t* test,  $n = 6$ ) that was maintained throughout the recording (Fig. 8*A*, middle

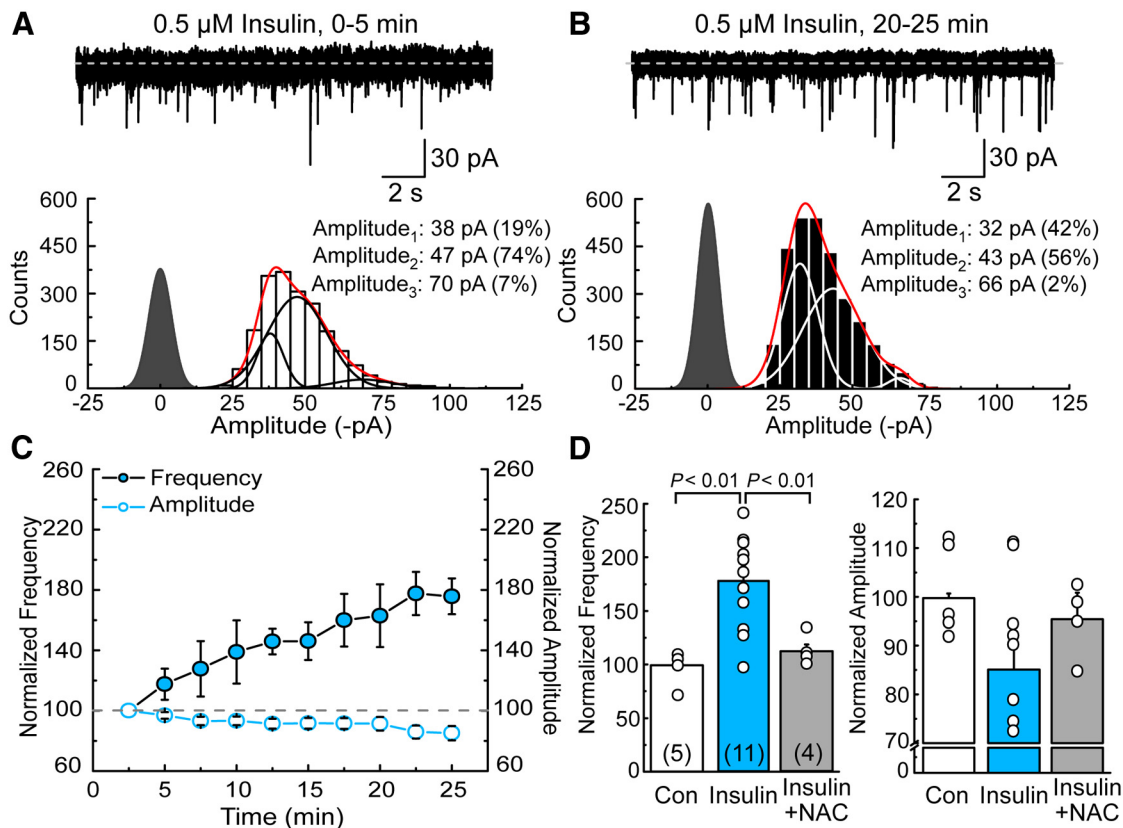


**Figure 7.** Insulin selectively increases the occurrence of inhibitory events of small amplitude. **A, B**, Top, mIPSCs from the same granule cell (cell #1503150007) at the beginning (0–5 min) and during (20–25 min) bath application with insulin (0.5  $\mu$ M). Bottom, Amplitude histograms comparing the data obtained at two time periods (i.e., 0–5 min, left; 20–25 min, right;  $n = 11$ ). Each was fit with the sum of three Gaussian functions (red line) with individual functions shown in either black (left) or white (right). **C**, Summary plot of the time course of mIPSC frequency (filled circle) and amplitude (open circle) during constant bath application with insulin. Data are mean  $\pm$  SEM. **D**, Bar graphs of maximal normalized frequency (left) and amplitude (right) obtained in the different recording conditions. Control, Con ( $n = 5$ ); *N*-acetylcysteine (1 mM), NAC ( $n = 4$ ). Statistical test was a one-way ANOVA with Tukey’s *post hoc* test. The frequency comparison of “Con” versus “Insulin + NAC” (**D**; left) was not significant and, for clarity, was not indicated in the figure. Amplitude comparisons were not significant ( $p = 0.26$ ; one-way ANOVA).

and bottom). Together, these data establish that insulin strengthens GABAergic synapses by recruiting  $\alpha 6$ -containing receptors.

Insulin has been shown to strengthen GABAergic synapses via a PI3-kinase pathway (Vetiska et al., 2007). To establish whether a similar pathway accounts for our observations, we examined the effect of the PI3-kinase inhibitor, wortmannin, on the ability of insulin to strengthen GABAergic synapses (Fig. 8D). As anticipated, internal patch perfusion of 1  $\mu$ M wortmannin completely blocked any change in mIPSC frequency and/or amplitude (Fig. 8D). mIPSC frequencies observed during the first (0–5 min) and last (20–25 min) 5 min were  $0.58 \pm 0.2$  Hz and  $0.60 \pm 0.2$  Hz, respectively ( $p = 0.53$ , paired Student’s *t* test;  $n = 6$ ). Additionally, the mIPSC amplitudes observed during the first (0–5 min) and last (20–25 min) 5 min were  $-46.6 \pm 1.9$  pA and  $-42.3 \pm 2.1$  pA, respectively ( $p = 0.07$ , paired Student’s *t* test;  $n = 6$ ). Together, these data show that wortmannin was effective in preventing the strengthening of GABAergic synapses by insulin. We therefore conclude that  $\alpha 6$ -selective strengthening of granule cell inhibitory synapses by insulin and ROS is mediated by activation of a wortmannin-sensitive, PI3-kinase pathway.

### Discussion

We report three key findings that have important ramifications for our understanding of inhibitory synapse strengthening. First, ROS strengthen cerebellar granule cell GABAergic synapses by recruiting GABARs of a different composition, in this case,  $\alpha 6$ -containing GABARs, rather than accumulating more of the

resident,  $\alpha 1$ -containing receptors. Second,  $\alpha 6$ -receptors are recruited to postsynaptic sites distinct from  $\alpha 1$ -receptors, implying that ROS strengthen only a subset of all possible inhibitory synapses. Third and finally, we reveal that insulin strengthens inhibitory GABAergic synapses of granule cells through this mechanism. Given the similarity to our recent findings on stellate cells, we propose that ROS uncover a novel mechanism by which inhibitory synapses are strengthened. In this case, GABARs that normally reside at inhibitory synapses, such as  $\alpha 1$ -receptors, form the hardwiring of neuronal circuits with receptors of a different subunit composition,  $\alpha 3$ -receptors in stellate cells or  $\alpha 6$ -receptors in granule cells, fulfilling a more prominent and unappreciated role in synapse strengthening. Because this mechanism is distinct from the predominant view of how inhibitory synapses are strengthened, our data suggest that more than one type of mechanism is responsible for strengthening inhibitory synapses in the adult CNS.

### GABA<sub>A</sub> receptor synapses are strengthened by more than one mechanism

Numerous studies have described inhibitory synapse strengthening in different CNS regions underpinning its importance as a pervasive regulator of neuronal circuits (Kittler and Moss, 2003; Luscher et al., 2011). Strengthening is thought to occur by the lateral diffusion of extrasynaptic GABARs (Thomas et al., 2005; Bogdanov et al., 2006), although it may also occur by direct insertion of receptors (Luscher et al., 2011). It is generally thought

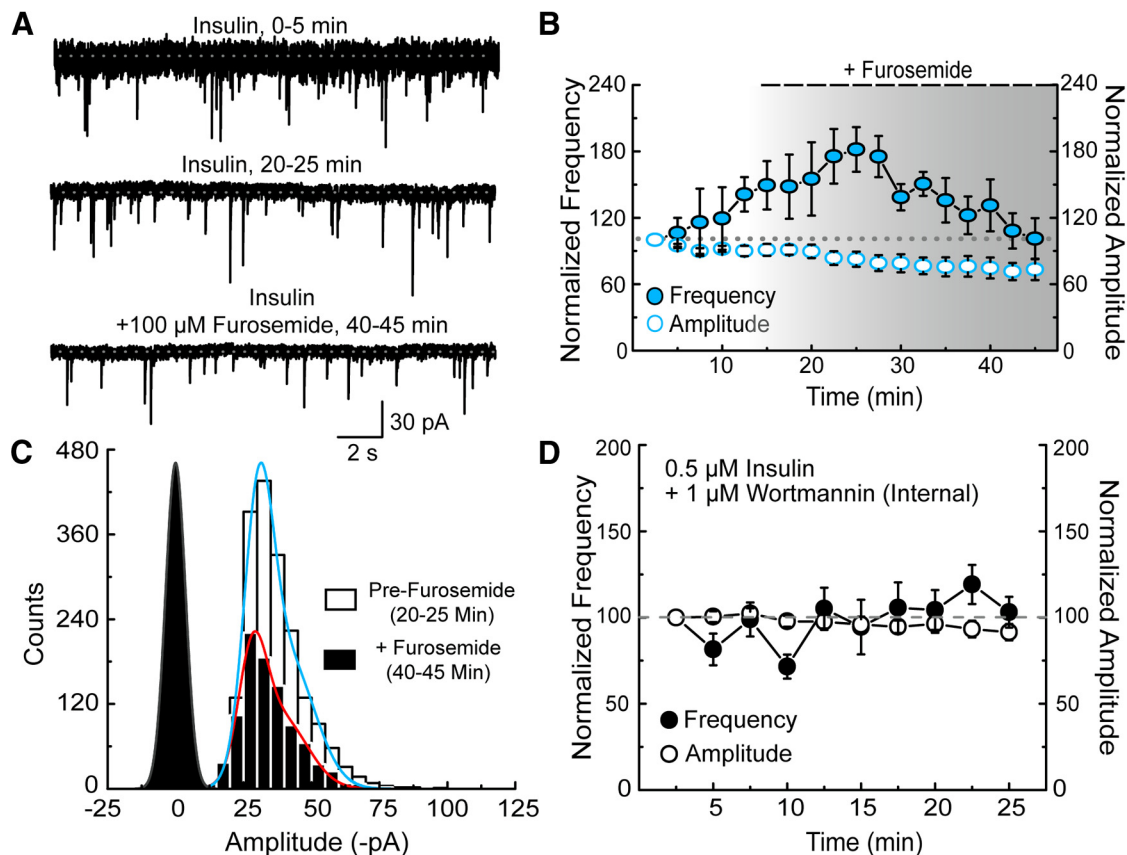


**Figure 8.** Synaptic strengthening induced by insulin is attenuated by pharmacological block of  $\alpha 6$ -containing GABA<sub>A</sub> receptors. **A**, Representative electrophysiological traces of a cerebellar granule cell in the presence of insulin ( $0.5 \mu\text{M}$ , cell #150319000) at three separate time points. **B**, Summary plot showing the time course of mIPSC frequency (filled cyan circle) and amplitude (open circle). Furosemide ( $100 \mu\text{M}$ ) was added 15 min after the start of the experiment. Insulin was present within the bath throughout the duration of the experiment. Gray gradient represents the gradual equilibration of furosemide in the bath. **C**, Amplitude distributions of mIPSCs from two time points ( $n = 6$ ). For clarity, only the summed Gaussian functions are shown (cyan represents Pre-Furosemide; red represents + Furosemide). **D**, Summary plot showing the time course of mIPSC frequency (filled circle) and amplitude (open circle) during internal perfusion of wortmannin ( $1 \mu\text{M}$ ) during continuous bath application of insulin ( $n = 6$ ). Data are mean  $\pm$  SEM.

that inhibitory synapse strengthening is due to an effect on pre-existing synapses rather than the recruitment of receptors to a subset of postsynaptic sites, as described here for  $\alpha 6$ -receptors (see also Accardi et al., 2014), or even to silent synapses (Inoue et al., 2013). The most compelling evidence favoring the idea that synapse strengthening is due to an accumulation of more receptors per synapse comes from electrophysiological measurements of inhibitory synaptic events (e.g., Otis et al., 1994; Wan et al., 1997; Nusser et al., 1998b; Thomas et al., 2005; Houston et al., 2008; Rannals and Kapur, 2011). In these examples, spontaneous and/or mini-events increased in amplitude, in marked contrast to our observations. Whether synapse strengthening also involves more than one type of  $\alpha$ -containing GABAR in these studies was not considered. Consequently, our observations described here on granule cells and elsewhere on stellate cells (Accardi et al., 2014) introduces an added complication for future studies to examine more closely. Whether  $\alpha 3$ - or  $\alpha 6$ -receptors of stellate or granule cells, respectively, are recruited into inhibitory synapses by lateral diffusion or by direct insertion also awaits future study. Together, however, the most parsimonious explanation of our data is that mROS uncover a novel mechanism by which inhibitory transmission can be strengthened. Moreover, given the emerging view that mROS lie at the center of many diverse biochemical pathways (Sena and Chandel, 2012), it is quite likely that strengthening of inhibitory synapses may be triggered by a myriad of signaling molecules that converge on this pathway.

### Insulin strengthens inhibitory GABAergic synapses in a subunit-dependent manner

Our data identify an unexpected causal relationship between insulin signaling, cytosolic ROS, and the level of GABAergic inhibition. Most strikingly, insulin receptor activation promotes an increase in GABAergic transmission by selectively recruiting  $\alpha 6$ -containing GABARs and having little or no effect on resident  $\alpha 1$ -receptors. Exactly how insulin and ROS achieve this remains to be studied in greater detail. Prior work on nonexcitable tissue, however, has shown that activation of the insulin receptor elevates cytosolic ROS by coupling to the plasma membrane-bound NADPH oxidase system (Goldstein et al., 2005). These events then play a key role in modifying the activity of a plethora of thiol-dependent regulatory proteins (Papaconstantinou, 2009). Interestingly, the inhibitory synapse scaffolding protein, gephyrin, is modified by changes in the ROS signaling molecule, nitric oxide, causing the S-nitrosylation of gephyrin to regulate GABAR synapse clustering (Dejanovic and Schwarz, 2014). However, because post-translational modification of gephyrin reduces the size of putative inhibitory synapses, and presumably weakens synapse strength (Dejanovic and Schwarz, 2014), these findings seem inconsistent with our observations showing that ROS strengthen GABAergic synapses. Clearly, more work is required to elucidate the biochemical events linking elevations

in cytosolic ROS to changes in efficacy of inhibitory synapses of granule cells.

Our imaging data also reveal the constitutive presence of a basal cytosolic ROS background in naive slices due to appreciable constitutive, genistein-sensitive tyrosine kinase activity (Fig. 6). It is still not clear whether this observation is due to elevated levels of circulating insulin, which can be 10–100 times higher in the CNS compared with plasma levels (Havrankova et al., 1978), or the action of other tyrosine kinase receptors. Assuming insulin is implicated, it would suggest that its local production in acutely isolated cerebellar slices is substantial, similar to recent findings in the cerebral cortex where GABAergic neurogliaform cells have been shown to be a major source of insulin (Molnár et al., 2014). Our data also reveal that a substantial population of granule cells respond to insulin through either changes in ROS (Fig. 6) or the recruitment of  $\alpha 6$ -containing GABARs (Fig. 8). Exactly how insulin signaling impacts granule cells and the cerebellar circuit is still unclear, although it may act, as with cortical neurogliaform cells (Molnár et al., 2014), to locally regulate neurotransmission and firing rates in response to fluctuations in circulating glucose. Given that local blood flow and glucose levels are tightly regulated by neurons and glial cells in close proximity (Attwell et al., 2010), it is tempting to speculate that the release and action of insulin are part of an overall homeostatic mechanism that ensures the efficient coupling of cellular metabolism to neuronal signaling in the cerebellum.

#### GABA<sub>A</sub> receptor heterogeneity and its role in synapse strengthening

Since the cloning studies in the 1990s, it has been well established that different brain regions, and even individual neurons, can express multiple GABAR isoforms, raising the question of the significance of this receptor heterogeneity. In the context of the present study, the role of several granule cell GABAR subtypes has been identified and is linked to constraining granule cell excitability and output to other cerebellar regions. Inhibitory transmission onto granule cells occurs via two distinct mechanisms (i.e., phasic and tonic inhibition), which represents signaling by synaptic and extrasynaptic receptors, respectively (Semyanov et al., 2004). Phasic inhibition is largely mediated by  $\alpha 1$ -containing GABARs (Nusser et al., 1998a), whereas tonic inhibition occurs by activation of  $\delta$ -containing GABARs (Nusser et al., 1996; Tia et al., 1996), which preferentially coassemble with  $\alpha 6$ -subunits (Nusser et al., 1996). Despite their presence at granule cell synapses (Nusser et al., 1996; Tia et al., 1996), the role fulfilled by  $\alpha 6/\gamma 2$  GABARs has been ill defined (Nusser et al., 1998a). Our study identifies an unexpected role for  $\alpha 6/\gamma 2$  GABARs that can enter inhibitory synapses under two conditions. First, in wild-type mice, elevations in ROS bring about a recruitment of  $\alpha 6/\gamma 2$  GABARs into postsynaptic sites. Second, in  $\delta$ -KO mice, our data suggest that  $\alpha 6/\gamma 2$  GABARs overpopulate postsynaptic sites and thus compete with the functional role usually assigned to  $\alpha 1$ -receptors. Morphological evidence supporting this prominent role of  $\alpha 6/\gamma 2$  GABARs in wild-type mice is lacking (Nusser et al., 1996, 1998a), presumably because normal tissue fixations techniques do not initiate the events that would permit their recruitment. In keeping with this, there is a similar lack of morphological evidence supporting a prominent role of  $\alpha 3$ -containing GABARs at stellate cell inhibitory synapses (Nusser et al., 1997). However, functional data have shown that  $\alpha 3$ -containing GABARs become the dominant synaptic receptor in stellate cells of  $\alpha 1$ -KO mice (Vicini et al., 2001; Accardi et al., 2014) and are the primary mediator of strengthening of wild-type

stellate cell synapses (Accardi et al., 2014), analogous to our observations on  $\alpha 6$ -receptors in granule cells. Whether our observations point to a more general role of other  $\alpha$ -containing GABARs elsewhere in the CNS remains to be established. However, given the value of targeting GABARs to treat many types of CNS disorders (Rudolph and Knoflach, 2011; Rudolph and Möhler, 2014), the occurrence of receptor heterogeneity in individual neurons may be exploited to develop subunit-specific compounds that are clinically relevant.

#### References

- Accardi MV, Daniels BA, Brown PM, Fritschy JM, Tyagarajan SK, Bowie D (2014) Mitochondrial reactive oxygen species regulate the strength of inhibitory GABA-mediated synaptic transmission. *Nat Commun* 5:3168. [CrossRef Medline](#)
- Attwell D, Buchan AM, Charpak S, Lauritzen M, Macvicar BA, Newman EA (2010) Glial and neuronal control of brain blood flow. *Nature* 468:232–243. [CrossRef Medline](#)
- Barnard EA, Skolnick P, Olsen RW, Möhler H, Sieghart W, Biggio G, Braestrup C, Bateson AN, Langer SZ (1998) International Union of Pharmacology: XV. Subtypes of gamma-aminobutyric acid A receptors: classification on the basis of subunit structure and receptor function. *Pharmacol Rev* 50:291–313. [Medline](#)
- Belelli D, Harrison NL, Maguire J, Macdonald RL, Walker MC, Cope DW (2009) Extrasynaptic GABAA receptors: form, pharmacology, and function. *J Neurosci* 29:12757–12763. [CrossRef Medline](#)
- Bogdanov Y, Michels G, Armstrong-Gold C, Haydon PG, Lindstrom J, Pangalos M, Moss SJ (2006) Synaptic GABAA receptors are directly recruited from their extrasynaptic counterparts. *EMBO J* 25:4381–4389. [CrossRef Medline](#)
- Dejanovic B, Schwarz G (2014) Neuronal nitric oxide synthase-dependent S-nitrosylation of gephyrin regulates gephyrin clustering at GABAergic synapses. *J Neurosci* 34:7763–7768. [CrossRef Medline](#)
- Draguhn A, Verdorn TA, Ewert M, Seeburg PH, Sakmann B (1990) Functional and molecular distinction between recombinant rat GABAA receptor subtypes by Zn<sup>2+</sup>. *Neuron* 5:781–788. [CrossRef Medline](#)
- Fritschy JM, Panzanelli P (2006) Molecular and synaptic organization of GABAA receptors in the cerebellum: effects of targeted subunit gene deletions. *Cerebellum* 5:275–285. [CrossRef Medline](#)
- Goldstein BJ, Mahadev K, Wu X, Zhu L, Motoshima H (2005) Role of insulin-induced reactive oxygen species in the insulin signaling pathway. *Antioxid Redox Signal* 7:1021–1031. [CrossRef Medline](#)
- Haas M, Forbush B 3rd (1998) The Na-K-Cl cotransporters. *J Bioenerg Biomembr* 30:161–172. [CrossRef Medline](#)
- Havrankova J, Schmechel D, Roth J, Brownstein M (1978) Identification of insulin in rat brain. *Proc Natl Acad Sci U S A* 75:5737–5741. [CrossRef Medline](#)
- Houston CM, Hosie AM, Smart TG (2008) Distinct regulation of beta2 and beta3 subunit-containing cerebellar synaptic GABAA receptors by calcium/calmodulin-dependent protein kinase II. *J Neurosci* 28:7574–7584. [CrossRef Medline](#)
- Inoue W, Baimoukhametova DV, Füzesi T, Wamsteeker Cusulin JI, Kolblinger K, Whelan PJ, Pittman QJ, Bains JS (2013) Noradrenaline is a stress-associated metaplastic signal at GABA synapses. *Nat Neurosci* 16:605–612. [CrossRef Medline](#)
- Kittler JT, Moss SJ (2003) Modulation of GABAA receptor activity by phosphorylation and receptor trafficking: implications for the efficacy of synaptic inhibition. *Curr Opin Neurobiol* 13:341–347. [CrossRef Medline](#)
- Korpi ER, Kuner T, Seeburg PH, Lüddens H (1995) Selective antagonist for the cerebellar granule cell-specific gamma-aminobutyric acid type A receptor. *Mol Pharmacol* 47:283–289. [Medline](#)
- Laurie DJ, Seeburg PH, Wisden W (1992a) The distribution of 13 GABAA receptor subunit mRNAs in the rat brain: II. Olfactory bulb and cerebellum. *J Neurosci* 12:1063–1076. [Medline](#)
- Laurie DJ, Wisden W, Seeburg PH (1992b) The distribution of thirteen GABAA receptor subunit mRNAs in the rat brain: III. Embryonic and postnatal development. *J Neurosci* 12:4151–4172. [Medline](#)
- Llinás RH (1969) Physiological and morphological organization of the cerebellar circuits in various vertebrates. In: *Neurobiology of cerebellar evolution and development* (Llinás R, ed), pp 43–73. Chicago: American Medical Association.

- Luscher B, Fuchs T, Kilpatrick CL (2011) GABAA receptor trafficking-mediated plasticity of inhibitory synapses. *Neuron* 70:385–409. [CrossRef Medline](#)
- Mahadev K, Zilbering A, Zhu L, Goldstein BJ (2001a) Insulin-stimulated hydrogen peroxide reversibly inhibits protein-tyrosine phosphatase 1b in vivo and enhances the early insulin action cascade. *J Biol Chem* 276:21938–21942. [CrossRef Medline](#)
- Mahadev K, Wu X, Zilbering A, Zhu L, Lawrence JT, Goldstein BJ (2001b) Hydrogen peroxide generated during cellular insulin stimulation is integral to activation of the distal insulin signaling cascade in 3T3-L1 adipocytes. *J Biol Chem* 276:48662–48669. [CrossRef Medline](#)
- Mapelli L, Solinas S, D'Angelo E (2014) Integration and regulation of glomerular inhibition in the cerebellar granular layer circuit. *Front Cell Neurosci* 8:55. [CrossRef Medline](#)
- May JM, de Haën C (1979) Insulin-stimulated intracellular hydrogen peroxide production in rat epididymal fat cells. *J Biol Chem* 254:2214–2220. [Medline](#)
- Mihalek RM, Banerjee PK, Korpi ER, Quinlan JJ, Firestone LL, Mi ZP, Lagenaar C, Tretter V, Sieghart W, Anagnostaras SG, Sage JR, Fanselow MS, Guidotti A, Spigelman I, Li Z, DeLorey TM, Olsen RW, Homanics GE (1999) Attenuated sensitivity to neuroactive steroids in gamma-aminobutyrate type A receptor  $\delta$  subunit knockout mice. *Proc Natl Acad Sci U S A* 96:12905–12910. [CrossRef Medline](#)
- Miller PS, Smart TG (2010) Binding, activation and modulation of Cys-loop receptors. *Trends Pharmacol Sci* 31:161–174. [CrossRef Medline](#)
- Minier F, Sigel E (2004) Positioning of the alpha-subunit isoforms confers a functional signature to gamma-aminobutyric acid type A receptors. *Proc Natl Acad Sci U S A* 101:7769–7774. [CrossRef Medline](#)
- Misgeld U, Deisz RA, Dodt HU, Lux HD (1986) The role of chloride transport in postsynaptic inhibition of hippocampal neurons. *Science* 232:1413–1415. [CrossRef Medline](#)
- Molnár G, Faragó N, Kocsis ÁK, Rózsa M, Lovas S, Boldog E, Báldi R, Csajbók É, Gardi J, Puskás LG, Tamás G (2014) GABAergic neurogliaform cells represent local sources of insulin in the cerebral cortex. *J Neurosci* 34:1133–1137. [CrossRef Medline](#)
- Momiyama A, Takahashi T (1994) Calcium channels responsible for potassium-induced transmitter release at rat cerebellar synapses. *J Physiol* 476:197–202. [CrossRef Medline](#)
- Moss SJ, Smart TG (2001) Constructing inhibitory synapses. *Nat Rev Neurosci* 2:240–250. [CrossRef Medline](#)
- Mukherjee SP, Lane RH, Lynn WS (1978) Endogenous hydrogen peroxide and peroxidative metabolism in adipocytes in response to insulin and sulfhydryl reagents. *Biochem Pharmacol* 27:2589–2594. [CrossRef Medline](#)
- Nakahiro M, Arakawa O, Narahashi T, Ukai S, Kato Y, Nishinuma K, Nishimura T (1992) Dimethyl sulfoxide (DMSO) blocks GABA-induced current in rat dorsal root ganglion neurons. *Neurosci Lett* 138:5–8. [CrossRef Medline](#)
- Nusser Z, Roberts JD, Baude A, Richards JG, Somogyi P (1995) Relative densities of synaptic and extrasynaptic GABAA receptors on cerebellar granule cells as determined by a quantitative immunogold method. *J Neurosci* 15:2948–2960. [Medline](#)
- Nusser Z, Sieghart W, Stephenson FA, Somogyi P (1996) The alpha 6 subunit of the GABAA receptor is concentrated in both inhibitory and excitatory synapses on cerebellar granule cells. *J Neurosci* 16:103–114. [Medline](#)
- Nusser Z, Cull-Candy S, Farrant M (1997) Differences in synaptic GABA(A) receptor number underlie variation in GABA mini amplitude. *Neuron* 19:697–709. [CrossRef Medline](#)
- Nusser Z, Sieghart W, Somogyi P (1998a) Segregation of different GABAA receptors to synaptic and extrasynaptic membranes of cerebellar granule cells. *J Neurosci* 18:1693–1703. [Medline](#)
- Nusser Z, Hájos N, Somogyi P, Mody I (1998b) Increased number of synaptic GABA(A) receptors underlies potentiation at hippocampal inhibitory synapses. *Nature* 395:172–177. [CrossRef Medline](#)
- Otis TS, De Koninck Y, Mody I (1994) Lasting potentiation of inhibition is associated with an increased number of gamma-aminobutyric acid type A receptors activated during miniature inhibitory postsynaptic currents. *Proc Natl Acad Sci U S A* 91:7698–7702. [CrossRef Medline](#)
- Papaconstantinou J (2009) Insulin/IGF-1 and ROS signaling pathway cross-talk in aging and longevity determination. *Mol Cell Endocrinol* 299:89–100. [CrossRef Medline](#)
- Payne JA (1997) Functional characterization of the neuronal-specific K-Cl cotransporter: implications for [K<sup>+</sup>]<sub>o</sub> regulation. *J Physiol* 273:C1516–C1525. [Medline](#)
- Persohn E, Malherbe P, Richards JG (1992) Comparative molecular neuroanatomy of cloned GABAA receptor subunits in the rat CNS. *J Comp Neurol* 326:193–216. [CrossRef Medline](#)
- Rannals MD, Kapur J (2011) Homeostatic strengthening of inhibitory synapses is mediated by the accumulation of GABA(A) receptors. *J Neurosci* 31:17701–17712. [CrossRef Medline](#)
- Rudolph U, Knoflach F (2011) Beyond classical benzodiazepines: novel therapeutic potential of GABAA receptor subtypes. *Nat Rev Drug Discov* 10:685–697. [CrossRef Medline](#)
- Rudolph U, Möhler H (2014) GABAA receptor subtypes: therapeutic potential in Down syndrome, affective disorders, schizophrenia, and autism. *Annu Rev Pharmacol Toxicol* 54:483–507. [CrossRef Medline](#)
- Rudolph U, Crestani F, Möhler H (2001) GABA(A) receptor subtypes: dissecting their pharmacological functions. *Trends Pharmacol Sci* 22:188–194. [CrossRef Medline](#)
- Semyanov A, Walker MC, Kullmann DM, Silver RA (2004) Tonic active GABA A receptors: modulating gain and maintaining the tone. *Trends Neurosci* 27:262–269. [CrossRef Medline](#)
- Sena LA, Chandel NS (2012) Physiological roles of mitochondrial reactive oxygen species. *Mol Cell* 48:158–167. [CrossRef Medline](#)
- Somogyi P, Fritschy JM, Benke D, Roberts JD, Sieghart W (1996) The gamma 2 subunit of the GABAA receptor is concentrated in synaptic junctions containing the alpha 1 and beta 2/3 subunits in hippocampus, cerebellum and globus pallidus. *Neuropharmacology* 35:1425–1444. [CrossRef Medline](#)
- Thomas P, Mortensen M, Hosie AM, Smart TG (2005) Dynamic mobility of functional GABAA receptors at inhibitory synapses. *Nat Neurosci* 8:889–897. [CrossRef Medline](#)
- Tia S, Wang JF, Kotchabhakdi N, Vicini S (1996) Developmental changes of inhibitory synaptic currents in cerebellar granule neurons: role of GABA(A) receptor alpha 6 subunit. *J Neurosci* 16:3630–3640. [Medline](#)
- Tretter V, Hauer B, Nusser Z, Mihalek RM, Höger H, Homanics GE, Somogyi P, Sieghart W (2001) Targeted disruption of the GABA(A) receptor  $\delta$  subunit gene leads to an up-regulation of gamma 2 subunit-containing receptors in cerebellar granule cells. *J Biol Chem* 276:10532–10538. [CrossRef Medline](#)
- Vetiska SM, Ahmadian G, Ju W, Liu L, Wymann MP, Wang YT (2007) GABAA receptor-associated phosphoinositide 3-kinase is required for insulin-induced recruitment of postsynaptic GABAA receptors. *Neuropharmacology* 52:146–155. [CrossRef Medline](#)
- Vicini S, Ferguson C, Prybylowski K, Kralic J, Morrow AL, Homanics GE (2001) GABA(A) receptor alpha1 subunit deletion prevents developmental changes of inhibitory synaptic currents in cerebellar neurons. *J Neurosci* 21:3009–3016. [Medline](#)
- Wall MJ, Usowicz MM (1997) Development of action potential-dependent and independent spontaneous GABAA receptor-mediated currents in granule cells of postnatal rat cerebellum. *Eur J Neurosci* 9:533–548. [CrossRef Medline](#)
- Wan Q, Xiong ZG, Man HY, Ackerley CA, Braunton J, Lu WY, Becker LE, MacDonald JF, Wang YT (1997) Recruitment of functional GABA(A) receptors to postsynaptic domains by insulin. *Nature* 388:686–690. [CrossRef Medline](#)
- Wozniak M, Rydzewski B, Baker SP, Raizada MK (1993) The cellular and physiological actions of insulin in the central nervous system. *Neurochem Int* 22:1–10. [CrossRef Medline](#)
- Zeng G, Quon MJ (1996) Insulin-stimulated production of nitric oxide is inhibited by wortmannin: direct measurement in vascular endothelial cells. *J Clin Invest* 98:894–898. [CrossRef Medline](#)